Solar spectral radiative forcing during the Southern African Regional Science Initiative

P. Pilewskie,[1] J. Pommier,[2] R. Bergstrom,[2] W. Gore,[1] S. Howard,[2] M. Rabbette,[2] B. Schmid,[2] P. V. Hobbs,[3] and S. C. Tsay[4]

Received 3 April 2002; revised 7 July 2002; accepted 8 July 2002; published 13 March 2003.

[1] During the dry season component of the Southern African Regional Science Initiative (SAFARI) in late winter 2000, the net solar spectral irradiance was measured at flight levels throughout biomass burning haze layers. From these measurements, the flux divergence, fractional absorption, instantaneous heating rate, and absorption efficiency were derived. Two cases are examined: on 24 August 2000 off the coast of Mozambique in the vicinity of Inhaca Island and on 6 September 2000 in a very thick continental haze layer over Mongu, Zambia. The measured absolute absorption was substantially higher for the case over Mongu where the measured midvisible optical depth exceeded unity. Instantaneous heating from aerosol absorption was 4 K d^{-1} over Mongu, Zambia and 1.5 K d^{-1} near Inhaca Island, Mozambique. However, the spectral absorption efficiency was nearly identical for both cases. Although the observations over Inhaca Island preceded the ''river of smoke'' from the southern African continent by nearly 2 weeks, the evidence here suggests a continental influence in the lower tropospheric aerosol far from source regions of burning. *INDEX TERMS:* 0305 Atmospheric Composition and Structure: Aerosols and particles (0345, 4801); 0342 Atmospheric Composition and Structure: Middle atmosphere—energy deposition; 0345 Atmospheric Composition and Structure: Pollution—urban and regional (0305); 0360 Atmospheric Composition and Structure: Transmission and scattering of radiation; 0394 Atmospheric Composition and Structure: Instruments and techniques; *KEYWORDS:* solar radiation, aerosols, climate, radiometric measurements

Citation: Pilewskie, P., J. Pommier, R. Bergstrom, W. Gore, S. Howard, M. Rabbette, B. Schmid, P. V. Hobbs, and S. C. Tsay, Solar spectral radiative forcing during the Southern African Regional Science Initiative, *J. Geophys. Res.*, *108*(D13), 8486, doi:10.1029/2002JD002411, 2003.

1. Introduction

[2] The Southern African Regional Science Initiative (SAFARI 2000) was conducted, in part, to study the regional influence on climate from biogenic, pyrogenic, and anthropogenic emission over the southern African continent (R. J. Swap et al., The Southern African Regional Science Initiative (SAFARI 2000): Dry-season field campaign: An overview, submitted to *South African Journal of Science*, 2002). The experimental phase of the program occurred at a time of heightened concern about the radiative impact of atmospheric aerosol particles on global climate change. The International Panel on Climate Change [*IPCC*, 1995, 2001] has identified aerosol radiative forcing as one of the major uncertainties in the global radiative energy budget. The role of black carbon, in particular, has been the focus of several recent studies [*Hansen et al.*, 2000; *Jacobson*, 2001] because the warming caused by the absorption of solar radiation by black carbon aerosols may be nearly equal in magnitude to the cooling caused by scattering of solar radiation by other aerosols.

[3] Quantifying the absorption of solar radiation by aerosols usually depends upon the inference of single scattering albedo from in situ measurements of aerosol light scattering and absorption, or on the inversion of lidar or solar photometric measurements. Absorption by aerosol layers is then determined by radiative transfer calculations, which also require knowledge of the scattering phase function and aerosol optical thickness. Optical thickness is the most accurately measured of these three parameters. Several sensitivity studies have shown a large disparity among various in situ and indirect determinations of single scattering albedo [*Russell et al.*, 2002; *Mlawer et al.*, 2000; *Halthore et al.*, 1998]. The scattering phase function, or its first moment, the asymmetry parameter, can be derived by only inverse methods, yet one of the properties of aerosol particles that affect the scattering phase function most strongly, shape, is often poorly characterized. Consequently, there is uncertainty associated with aerosol absorption, especially in dusty environments [cf. *Dubovik et al.*, 2000, 2002].

[4] During SAFARI 2000 the NASA Ames Research Center Radiation Group deployed Solar Spectral Flux

[1]Earth Science Division, NASA Ames Research Center, Moffett Field, California, USA.
[2]Bay Area Environmental Research Institute, Sonoma, California, USA.
[3]Department of Atmospheric Sciences, University of Washington, Seattle, Washington, USA.
[4]NASA Goddard Space Flight Center, Greenbelt, Maryland, USA.

0148-0227/03/2002JD002411$09.00

Radiometers (SSFR) on the NASA ER-2 (M. D. King et al., Remote sensing of smoke, land and clouds from the NASA ER-2 during SAFARI 2000, submitted to *Journal of Geophysical Research*, 2002, hereinafter referred to as King et al., submitted manuscript, 2002) and on the University of Washington Convair-580 [*Sinha et al.*, 2003]. On both aircraft, the SSFR made simultaneous measurements of upwelling and downwelling solar spectral irradiance. On the ER-2 the SSFR was used to characterize the solar spectral radiation distribution in the upper atmosphere, providing a valuable source of data for comparison with spaceborne Earth radiation budget sensors, such as the Clouds and the Earth's Radiant Energy System (CERES) [*Wielicki et al.*, 1996]. The Convair-580 thoroughly profiled the lower troposphere, thus providing solar radiation "closure" in vertical columns containing elevated levels of aerosol loading. The focus of this paper is on two Convair-580 radiation profiles, on 24 August and 6 September, off the coast of Mozambique and over Zambia, respectively. We derive the solar spectral flux divergence for these cases and the layer absorption efficiency. The methods described here provide a means for quantifying aerosol absorption more directly than those described above. A companion study by *Bergstrom et al.* [2003] describes detailed radiative transfer analysis of these cases and comparisons with SSFR.

2. Instrumentation

2.1. The Solar Spectral Flux Radiometer

[5] The SSFR is a moderate resolution flux (irradiance) spectrometer covering the wavelength range from 300 to 1700 nm. The SSFR is comprised of an identical pair of Zeiss Monolithic Miniature Spectrometer Modules (MMS 1 and MMS NIR) for simultaneous zenith and nadir viewing. The MMS-1 is equipped with a flat-field, 366 1/mm grating and a Hamamatsu Si linear diode array detector. We apply thermal control to the MMS-1 module, holding temperature at 27°C ± 0.3°C. The MMS-NIR has a 179 1/mm flat-field grating with a 128-element InGaAs linear diode array, thermoelectrically cooled to 0°C. Spectral resolution is 9 nm for the MMS-1 and 12 nm for the MMS-NIR. The light collector is a scaled version of the optical collector used for the spectral diffuse/global irradiance meter designed by *Crowther* [1997]. It is a spectralon integrating sphere with a conical baffle, also made of spectralon, and a barium sulfate coated knife edge. The design for this sphere has been tested for angular response by computer simulation and in the laboratory. It shows a high degree of linearity with cosine of incidence angle to values as low as 0.1. The light collector is protected in flight by a water-free quartz hyperdome. At the base of the spectralon sphere is a high-grade custom-made fiber optic bundle (Ceram Optec) which is bifurcated to transmit the incident light to the two spectrometer input slits for visible and near-infrared detection. The data acquisition and control system is driven by a 100 MHz 486 PC in a PC104 format. The dynamic resolution is 15 bits full range. Sampling resolution is approximately 3.25 nm. Integration time for each of the spectrometers is nominally 100 ms. Spectral sampling rate is approximately 1 Hz. Data are recorded on a compact 225 Mb PCMCIA flash memory card.

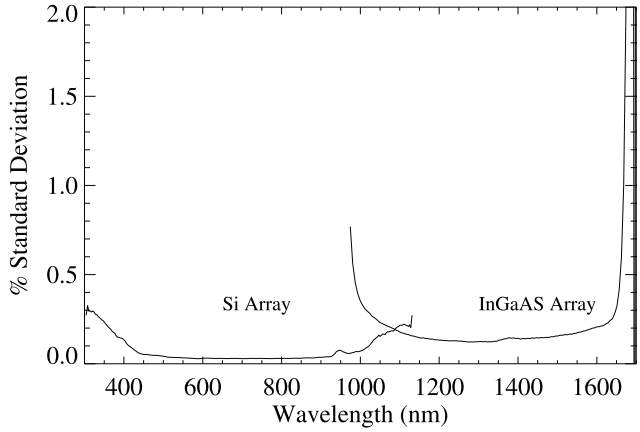

Figure 1. The relative standard deviation from a set of 100 SSFR spectra of a stable NIST calibration source.

2.2. Calibration of SSFR

[6] The SSFR is calibrated for wavelength, angular response, and absolute spectral power. Spectral calibration is achieved by referencing to the HeNe laser line at 632.8 nm, a temperature stabilized laser diode line at 1298 nm, and several line sources from Hg, Xe, and Ar lamps. The spectral power calibration was conducted prior to the SAFARI campaign using a NIST secondary standard lamp at the NASA Ames Airborne Sensor Facility Laboratory and in our laboratory using a LI-COR Field Calibrator. The NIST standard is operated at 1000 W and viewed at 50 cm. The LI-COR units are fully enclosed devices (200 W lamps with exit aperture at 20 cm) which are more suitable for field use. In the field, we calibrate the SSFR before and after flights using the same portable LI-COR devices to monitor the stability of the SSFR over the duration of the experiment.

[7] Measures of instrument stability can be seen in the spectral distribution of relative standard deviation in a collection of 100 calibration spectra (Figure 1) and a comparison of predeployment and postdeployment instrument response spectra (Figure 2). Over most of the active spectral range the short-term stability, or precision, depicted in Figure 1, is better than 0.1% for the Si detector array and better than 0.2% for the InGaAs detector array. At the short and long wavelength detection limit for each array, the stability is worse because of reduced detector quantum efficiency and stray light effects. The longer-term stability shown by the comparison of predeployment and postdeployment response function comparisons is around 0.5% for the Si array and 0.75% for InGaAs, with similar falloff at the detection limits. The data presented in this paper are in the range 350–1650 nm, excluding bands with lowest signal-to-noise ratio.

[8] The absolute accuracy of SSFR irradiance spectra depends mostly on the accuracy of the transfer standard. The error over our spectral range for the NIST standard used to calibrate the SSFR was between 1% and 3%. The LI-COR calibrator lists a 3% uncertainty across the spectrum. Additional error occurs during aircraft operations because of

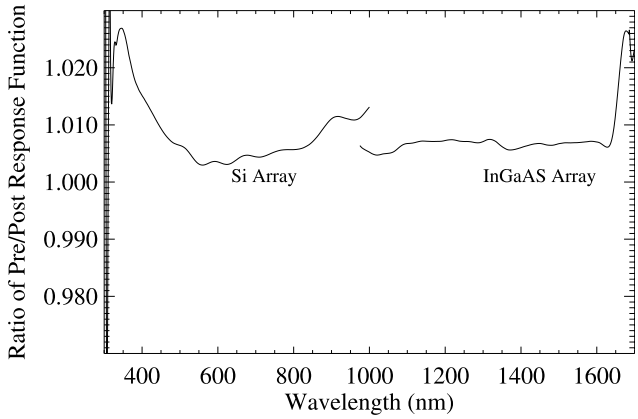

Figure 2. A comparison between predeployment and postdeployment SSFR response functions.

aircraft pitch and roll. Corrections are applied to the downwelling flux to correct for these effects.

3. Spectral Irradiance

[9] Case study days on 24 August and 6 September provide examples of the large contrast in aerosol loading that were encountered during SAFARI 2000. On 24 August, the Convair-580 flew a profile of stacked, level legs over Inhaca Island off the Mozambique coast in a relatively pristine maritime air mass (Figure 3a). By contrast, on 6 September the Convair-580 flew level legs at 175 m (878 hPa) and 3000 m (574 hPa), respectively, over the Mongu, Zambia airport in extremely hazy conditions (Figure 3b). In this section, we will examine the influence of aerosol scattering and absorption on the measured spectral irradiance.

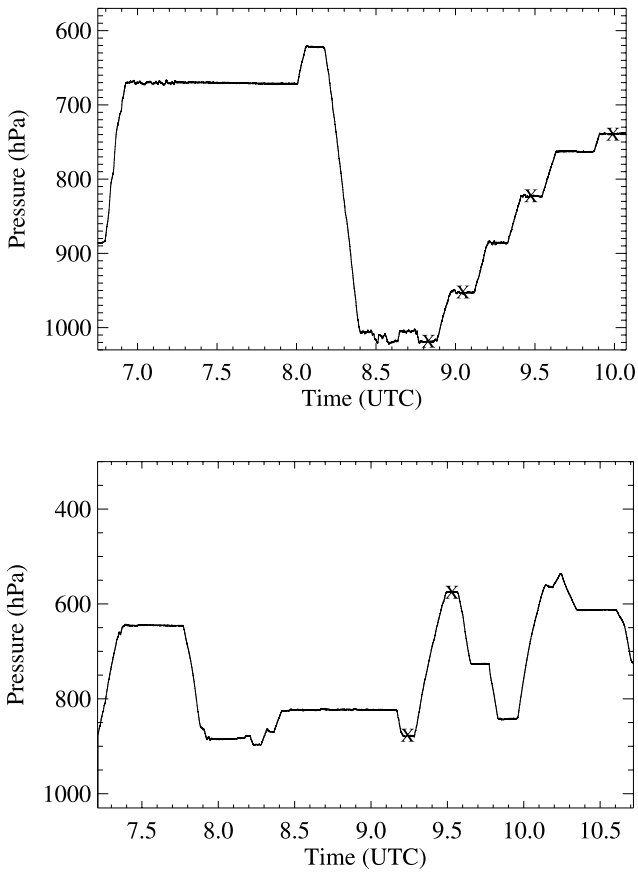

Figure 3. (a) University of Washington Convair-580 flight profile on 24 August 2000 near Inhaca Island, Mozambique. "X" indicates the flight legs analyzed in this study. (b) University of Washington Convair-580 flight profile on 6 September 2000. "X" identifies two legs flown over the Mongu, Zambia airport under extremely hazy conditions.

3.1. 24 August: Inhaca Island, Mozambique

[10] The Convair-580 mission on 24 August included a vertical ascent off the coast of Mozambique in the vicinity of Inhaca island. The duration of the level flight legs was between 5 and 10 min. SSFR upwelling and downwelling averaged over four of the legs are shown in the top panel of Figure 4. In cloud-free conditions, the directly transmitted flux comprises a large fraction of the downwelling irradiance. We have corrected downwelling irradiance for aircraft attitude in the following manner: we determine the cosine of solar zenith angle with respect to our sensor (μ') by a Eulerian transformation to an aircraft-based coordinate system dependent on aircraft pitch, roll, and heading. Wavelength dependent corrected flux (F_c) is determined by

$$F_c(\lambda) = \mu_o t(\lambda) F(\lambda)/\mu' + (1 - t(\lambda))F(\lambda) \quad (1)$$

where μ_o is the cosine of the solar zenith angle and $t(\lambda)$ is the wavelength dependent direct transmission determined

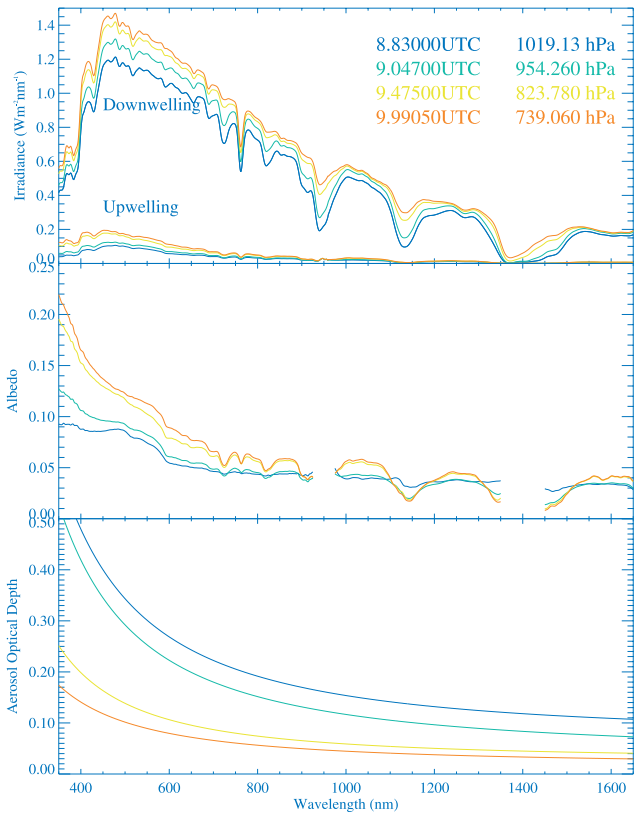

Figure 4. Top panel: upwelling and downwelling spectra from four flight legs in the vicinity of Inhaca Island, Mozambique on 24 August. Middle panel: albedo spectra from the same profile. Bottom panel: corresponding aerosol optical depths.

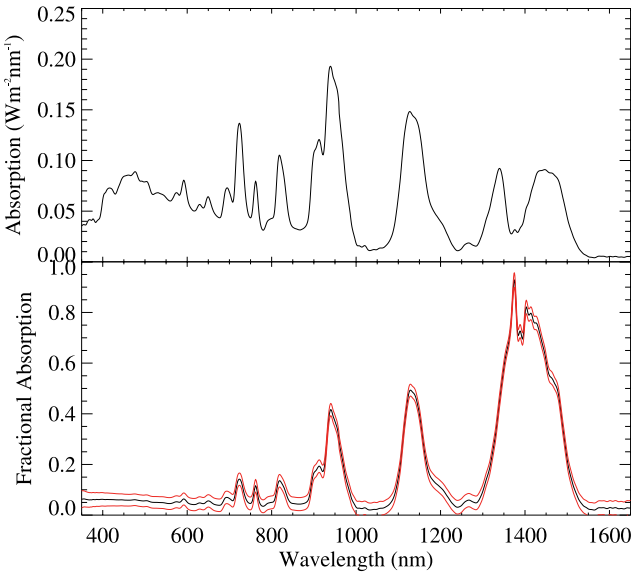

Figure 5. Upper panel: the spectral flux divergence (absorption) between the highest and the lowest flight legs in the 24 August flight profile in the vicinity of Inhaca Island. Lower panel: fractional absorption from the same case. Red curves indicate the range of uncertainty.

by the aerosol and molecular scattering and absorption optical depth. An offset in the mounting of a light collector or uncertainties in the navigational parameters will lead to errors in the corrected flux. To reduce these uncertainties we allow for a range of error in pitch, roll, and heading, and solve for the set that minimizes differences in corrected flux in a least squares sense. The uncertainty associated with navigational correction is estimated to be 2%.

[11] The spectral albedo, $a(\lambda)$, at each flight level is given by the ratio of upwelling irradiance, $F_{\uparrow}$, to downwelling irradiance, $F_{\downarrow}$, and is shown in the middle panel of Figure 4. Gaps in the albedo spectra are due to low signal to noise in the upwelling irradiance in the 940 nm water vapor band and saturation in the 1400 nm water vapor band. The aerosol optical depths from the 14 channel Ames Airborne Tracking Sun photometer (AATS-14) flown on the same aircraft are shown in the lower panel in Figure 4. Continuous curves are derived by using a quadratic fit to 12 of the 14 AATS channels [*Schmid et al.*, 2003]. These data are used to determine the fraction of downwelling irradiance in the direct beam for the correction defined in (1).

[12] The net flux at any level is defined as the difference between downwelling and upwelling irradiance:

$$F_{net} = F_{\downarrow} - F_{\uparrow} \tag{2}$$

and the spectral flux divergence, or absorption, A, in a layer is defined as the difference between net flux above and below a layer:

$$A(\lambda) = \left(F_{\downarrow} - F_{\uparrow}\right)_2 - \left(F_{\downarrow} - F_{\uparrow}\right)_1 \tag{3}$$

where subscripts 2 and 1 denote upper and lower flight levels, respectively. Finally, we determine fractional absorption, α, by normalizing the layer absorption by the downwelling flux incident at the top of the layer:

$$\alpha = \frac{\left(F_{\downarrow} - F_{\uparrow}\right)_2 - \left(F_{\downarrow} - F_{\uparrow}\right)_1}{F_{\downarrow 2}} \tag{4}$$

[13] Figure 5 shows the absorption (upper panel) and fractional absorption (lower panel) for the layer between the highest and lowest flight legs of the Inhaca Island profile. Note that the largest absolute absorption occurs in the 940 nm water band. In a fractional sense, absorption in the 1400 nm band is greatest, compared to what is incident on the layer. The influence of aerosol is seen mostly in the visible part of the spectrum, at wavelengths less than 700 nm, where gas absorption is less than in the near-infrared. In the lower panel of Figure 5 it is evident that the aerosol fractional absorption in the visible is nearly constant at 0.05.

[14] The significance of this level of absorption can be determined by estimating the aerosol single scattering albedo (ϖ_o) necessary to produce the absorption in Figure 5. Assuming single scattering, an approximate formula relating layer fractional absorption to aerosol single scattering albedo is:

$$\alpha = \frac{(1-\varpi_o)\left(1-e^{-\tau/\mu o}\right)\left(1-e^{-d\tau}\right)a_S\left\{e^{-\tau/\mu o} + \varpi_o f\left(1-e^{-\tau/\mu o}\right)\right\}}{1 - a_s\varpi_o b\left(1-e^{-\tau/\mu o}\right)}. \tag{5}$$

Here τ is the combined aerosol and molecular scattering optical depth, a_S is the albedo at the lower level, f and b are the forward and backscattering fractions, respectively, and d is the diffusivity factor. The fractions of scattered light in the forward and back directions are functions of asymmetry parameter [*Wiscombe and Grams*, 1976]; since fractional absorption depends only weakly on asymmetry parameter [*Bergstrom et al.*, 2003] we assume a constant value of 0.7 and diffusivity is assumed to be 1.5 [*Goody*, 1964]. We solve for single scattering albedo by minimizing the least squares difference between measured and modeled fractional absorption.

[15] The derived spectrum for aerosol single scattering albedo is shown in Figure 6 along with uncertainty bounds determined mostly by the error in fractional absorption. The decrease in single scattering albedo with wavelength is consistent with absorption by elemental carbon and in general agreement with the more detailed analyses discussed in a companion study by *Bergstrom et al.* [2003]. It is also consistent with but somewhat lower than the spectral variation of single scattering albedo for biomass burning and urban/industrial aerosol as reported in the analysis of the large global network of AERONET Sun photometers [*Dubovik et al.*, 2002]. The dashed curve in Figure 6 is the *Dubovik et al.* [2002] retrieved single scattering albedo from biomass burning aerosol over African savanna. Note, however, the large spread in uncertainty, especially at longer wavelengths where the range of retrieved single scattering albedo lies between 0.9 and 0.6. Furthermore, the retrieved single scattering albedo represents a column average and is not representative of individual aerosol particles. Thus, we recommend using the

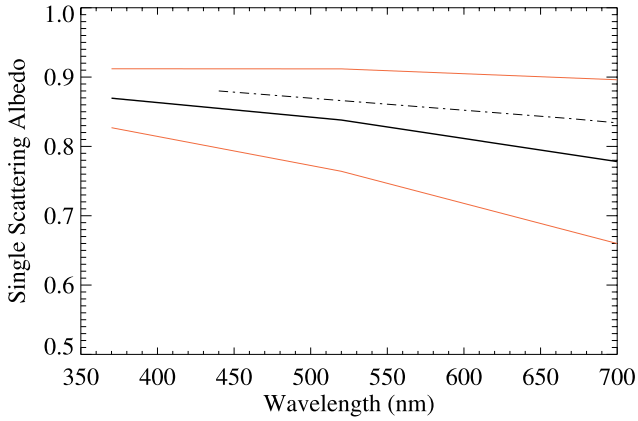

Figure 6. The retrieved single scattering albedo based upon the fractional absorption in Figure 5. Red curves indicate range of uncertainty. The dashed curve is retrieved single scattering albedo from biomass burning aerosol over African savanna [*Dubovik et al.*, 2002].

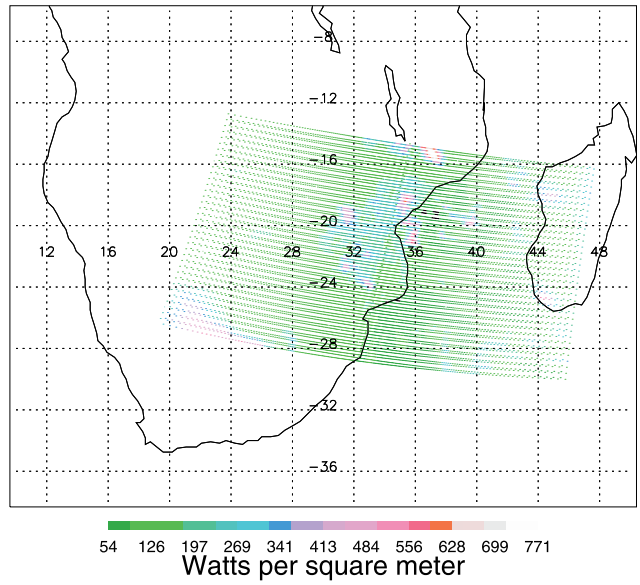

Figure 7. CERES shortwave reflected irradiance over southern Africa on 24 August 2000.

absorption spectra in Figure 5 to constrain a radiative transfer model rather than stipulating a column averaged single scattering albedo.

3.1.1. Comparison With CERES

[16] The CERES is a key component of the Earth Observing System (EOS) program. The first CERES instrument was launched from Japan, on 27 November 1997, as part of the Tropical Rainfall Measuring Mission (TRMM). Two more CERES instruments (FM1 and FM2) were launched into polar orbit on board the EOS Terra satellite on 18 December 1999. CERES products include both solar-reflected and Earth-emitted radiation from the top of the atmosphere to the Earth's surface. The CERES instrument provides radiometric measurements of the Earth's atmosphere from three broadband channels: 0.3–5.0, 8–12, and 0.3 to >100 μm. During SAFARI 2000 there were a number of coordinated ER-2 flights and Terra satellite overpasses (King et al., submitted manuscript, 2002). Figure 7 shows a sample of the shortwave reflected radiation obtained with the FM2 CERES instrument onboard the Terra platform on 24 August 2000, as it flew over the southern and eastern regions of Africa. The FM2 instrument operated almost continuously in the cross-track scan mode during August 2000.

[17] Figure 8 shows the SSFR downwelling and upwelling spectra from the ER-2 at the time of the Terra overpass. Included in the plot is a model (MODTRAN 4) calculation of spectral irradiance at the ER-2 flight altitude of 20 km using a sea surface albedo derived from the Convair-580 SSFR spectra at the lowest flight level. The agreement between measured and modeled downwelling spectra is rather good, but there is clearly a mismatch in the upwelling spectra because the broad field of view of the SSFR at 20 km includes nearly half land scene (the overpass site was just off the east coast of southern Africa). Likewise, comparison between CERES and integrated SSFR upwelling flux suffers from the same scene mixing. The CERES shortwave reflected flux at this time was 100 W m^{-2}, compared to an integrated SSFR upwelling value of 140 W m^{-2}. The CERES product converts a radiance measurement over a scene location to irradiance by means of a bidirectional reflectance function. Reconciliation of these data with SSFR upwelling irradiance will require a convolution of the CERES scene with the SSFR footprint.

3.2. 6 September: Mongu, Zambia

[18] On 6 September 2000, the Convair-580 flew two stacked level legs over Mongu, Zambia during an intense haze episode. SSFR downwelling and upwelling irradiance spectra from this case are illustrated in Figure 9, along with spectral albedo, and AATS optical depths. The influence of this massive optically thick haze layer is evident in the reduced near-infrared reflectance compared to the near-surface reflectance and suggests very strong absorption in the layer. The upper panel in Figure 10 shows the spectral absorption for the layer. The solid curve is total absorption; by interpolating across the various near-infrared gaseous absorption bands, we can estimate the aerosol contribution to the

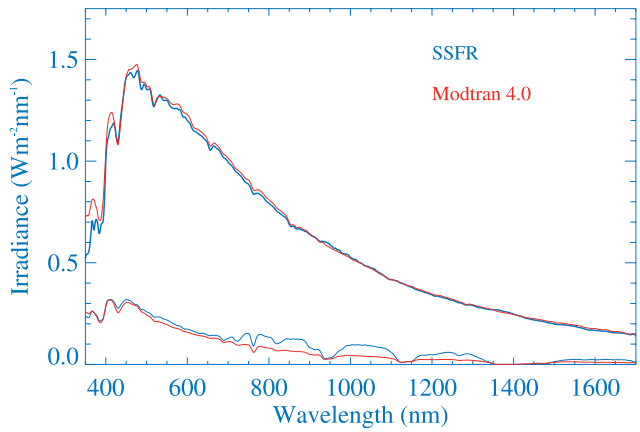

Figure 8. Comparison between measured (blue) and modeled (red) downwelling and upwelling spectral irradiance at ER-2 altitude (20 km) during the CERES overpass on 24 August 2000.

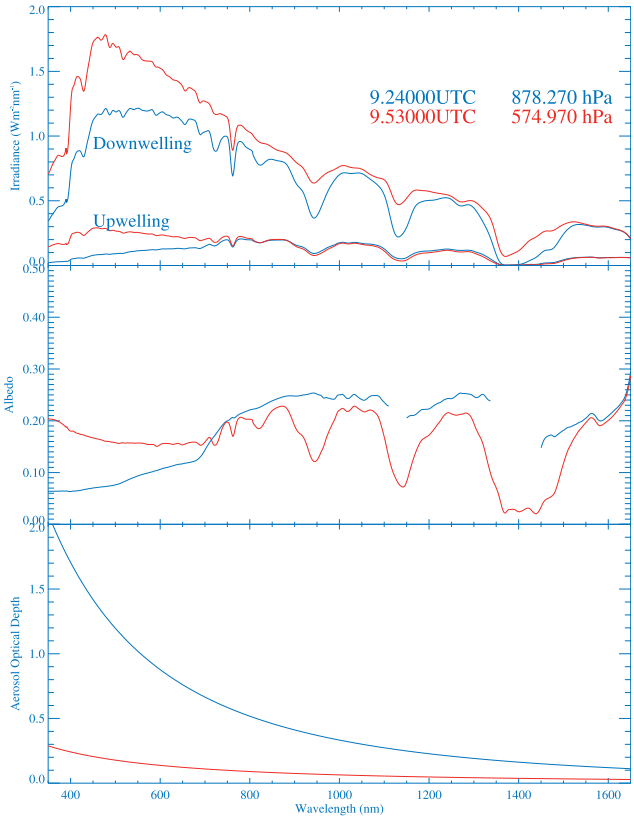

Figure 9. Top panel: upwelling and downwelling spectra from two flight legs over Mongu, Zambia on 6 September. Middle panel: albedo spectra from the same profile. Bottom panel: corresponding aerosol optical depths.

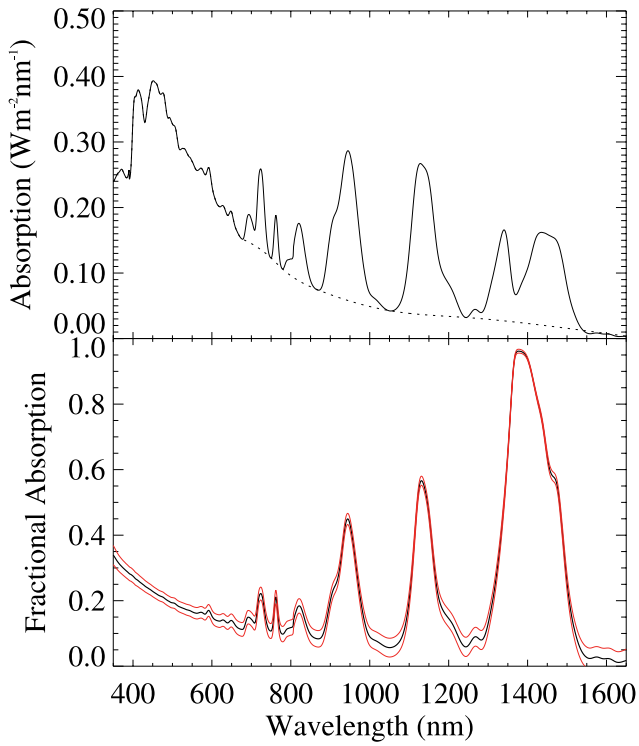

Figure 10. Upper panel: spectral flux divergence (absorption) between the high and the low flight legs in the 6 September flight profile over Mongu, Zambia. The dashed curve represents the aerosol absorption "continuum." Lower panel: fractional absorption from the same case. Red curves indicate the range of uncertainty.

absorption, which is depicted by the dashed curve in Figure 10. The integrated absorption due to this aerosol "continuum" is 138 W m^{-2}; the aerosol plus gas absorption is 199 W m^{-2}. The integrated downwelling irradiance at the top of the layer was 1051 W m^{-2} so the integrated fractional absorption by the thick haze layer was 0.13. The instantaneous heating rate in the layer, dT/dt, given by [e.g., *Hobbs*, 2000]

$$\frac{dT}{dt} = \frac{1}{gC_p}\frac{dF_{NET}}{dp}, \qquad (6)$$

(g is the acceleration due to gravity, C_p the specific heat of air at constant pressure, and dF_{NET}/dP the radiative flux divergence) was 4 K d^{-1} from aerosol and 5.8 K d^{-1} from aerosol and gas combined. Although substantial, the heating was considerably less than the heating measured in the plume from the Kuwait oil fires which approached 25 K d^{-1} [*Pilewskie and Valero*, 1992]. The instantaneous heating due to aerosol on 24 August, by contrast, was 1.5 K d^{-1}. The approximate single scattering formula (5) for deriving single scattering albedo is not applied here because the layer was too thick. *Bergstrom et al.* [2003] derive single scattering for this case by using a sophisticated multistream radiative transfer model.

3.3. Aerosol Forcing Efficiency

[19] *Bergstrom et al.* [2003] determined the radiative forcing for 24 August and 6 September cases by subtracting a model-derived aerosol-free net flux from the measured net flux above and below the haze layers. The magnitude of aerosol spectral radiative forcing at the surface was similar to that reported by *Meywerk and Ramanathan* [1999] and by *Bush and Valero* [2002] during the Indian Ocean Experi-

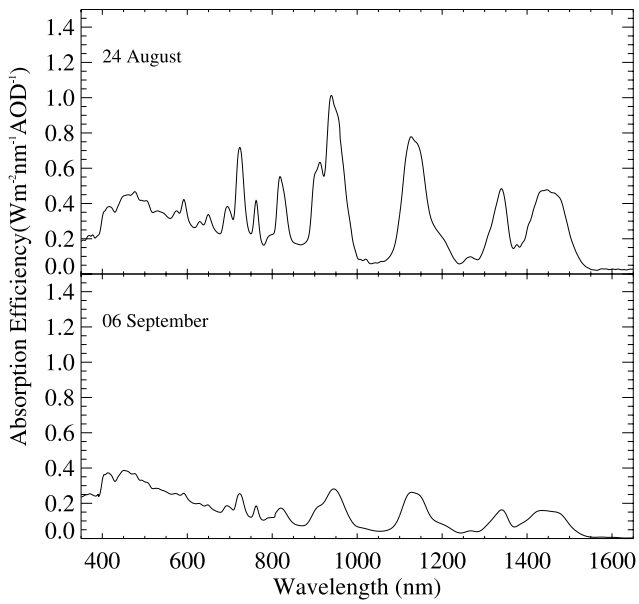

Figure 11. Spectral absorption efficiency for the 24 August and 6 September cases.

ment (INDOEX). The difference between top-of-atmosphere aerosol forcing and surface forcing is related to the absorption in the layer. We define aerosol absorption efficiency as the ratio of layer absorption ($A(\lambda)$ from (3)) divided by the aerosol optical depth at 500 nm. The results for both the 24 August case and the 6 September case are shown in Figure 11. The absorption efficiencies for the two cases are similar, even though the loading in Mongu (6 September) was far more severe.

[20] The spectra shown in Figure 11 compare favorably with the difference between TOA forcing and the surface forcing reported by *Bergstrom et al.* [2003], as expected. Indeed, outside of the gas absorbing bands, the difference between TOA and surface forcing should be equivalent to layer absorption. The focus of this study has been on the direct radiative effects of aerosol absorption and scattering. However, it has shown that absorbing aerosols can influence the formation and maintenance of clouds and thus induce an indirect effect on climate forcing [e.g., *Ackerman et al.*, 2000].

4. Summary

[21] During the SAFARI 2000 dry season campaign we measured the upwelling and downwelling solar spectral flux in the lower troposphere to determine the radiative forcing by aerosol layers. The flux, net flux, flux divergence, and relative absorption spectra were derived from above and below haze layers encountered on 24 August 2000 off the coast of Mozambique and on 6 September 2000 over Mongu, Zambia. Unique instrumentation and flight planning was key to deriving aerosol absorption and heating rates directly from measurements. Although the flights over Inhaca Island occurred in less hazy conditions than those encountered in Mongu, the efficiency of aerosol absorption (defined by normalization to 500 nm aerosol optical thickness) were nearly identical and suggests the presence of a continental influence over the whole region even before the more dramatic ''river of smoke'' event which occurred in early September (Annegarn et al., ''The river of smoke'': Characteristics of the southern African springtime biomass burning haze, submitted to *Journal of Geophysical Research*, 2002).

[22] **Acknowledgments.** We thank Larry Pezzolo for his technical support during the preparation and deployment phases of SAFARI 2000. The efforts of the University of Washington NASA ER-2 flight teams were crucial toward the success of the mission and we are grateful to them. We also thank two anonymous reviewers for their insightful comments and recommendations for improving the manuscript.

References

Ackerman, A., et al., Reduction of tropical cloudiness by soot, *Science*, *288*, 1042–1047, 2000.

Bergstrom, R. W., P. A. Pilewski, B. Schmid, and P. B. Russell, Estimates of the spectral aerosol single scattering albedo and aerosol radiative effects during SAFARI 2000, *J. Geophys. Res.*, *108*, doi:10.1029/2002JD002435, in press, 2003.

Bush, B. C., and F. P. J. Valero, Spectral aerosol radiative forcing at the surface during the Indian Ocean Experiment (INDOEX), *J. Geophys. Res.*, *107*(D19), 8003, doi:10.1029/2000JD000020, 2002.

Crowther, B. G., The design, construction, and calibration of a spectral diffuse global irradiance meter, Ph.D. thesis, 140 pp., Univ. of Arizona, Tucson, Ariz., 1997.

Dubovik, O., A. Smirnov, B. N. Holben, M. D. King, Y. J. Kaufman, T. F. Eck, and I. Slutsker, Accuracy assessments of aerosol optical properties retrieved from AERONET sun and sky-radiance measurements, *J. Geophys. Res.*, *105*, 979–980, 2000.

Dubovik, O., B. N. Holben, T. F. Eck, A. Smirnov, Y. J. Kaufman, M. D. King, D. Tanre, and I. Slutsker, Variability of absorption and optical properties of key aerosol types observed in worldwide locations, *J. Atmos. Sci.*, *59*, 590–608, 2002.

Goody, R. M., *Atmospheric Radiation*, Clarendon, Oxford, England, 1964.

Halthore, R. N., et al., Models overestimate diffuse clear-sky surface irradiance: A case for excess atmospheric absorption, *Geophys. Res. Lett.*, *25*, 3591–3594, 1998.

Hansen, J., et al., Global warming in the twenty-first century: An alternative scenario, *Proc. Natl. Acad. Sci. U. S. A.*, *97*, 9857–9880, 2000.

Hobbs, P. V., *Introduction to Atmospheric Chemistry*, Cambridge Univ. Press, New York, 2000.

Intergovernmental Panel on Climate Change (IPCC), *Climate Change, 1994: Radiative Forcing of Climate Change and an Evaluation of IPCC IS92 Emission Scenarios*, 339 pp., Cambridge Univ. Press, New York, 1995.

Intergovernmental Panel on Climate Change (IPCC), *Climate Change 2001: The Scientific Basis*, 881 pp., Cambridge Univ. Press, New York, 2001.

Jacobson, M. Z., Strong radiative heating due to the mixing state of black carbon in atmospheric aerosols, *Nature*, *409*, 695–697, 2001.

Meywerk, J., and V. Ramanathan, Observations of the spectral clear-sky aerosol forcing over the tropical Indian Ocean, *J. Geophys. Res.*, *104*, 24359–24370, 1999.

Mlawer, E. J., P. D. Brown, S. A. Clough, L. C. Harrison, J. J. Michalsky, P. W. Kiedron, and T. Shippert, Comparison of spectral direct and diffuse solar irradiance measurements and calculations for cloud-free conditions, *Geophys. Res. Lett.*, *27*, 2653–2656, 2000.

Pilewskie, P., and F. P. J. Valero, Radiative effects of the smoke from the Kuwait oil fires, *J. Geophys. Res.*, *97*, 14541, 1992.

Russell, P. B., et al., Comparison of aerosol single scattering albedos derived by diverse techniques in two North Atlantic experiments, *J. Aerosol Sci.*, *59*(3), 609–619, 2002.

Schmid, B., et al., Coordinated airborne, spaceborne, and ground-based measurements of massive, thick aerosol layers during the dry season in Southern Africa, *J. Geophys. Res.*, *108*, doi:10.1029/2002JD002297, in press, 2003.

Sinha, P., P. V. Hobbs, R. J. Yokelson, I. Bertschi, D. R. Blake, I. J. Simpson, S. Gao, T. L. Kirchstetter, and T. Novakov, Emissions of trace gases and particles from savanna fires in southern Africa, *J. Geophys. Res.*, *108*, doi:10.1029/2002JD002325, in press, 2003.

Wielicki, B. A., B. R. Barkstrom, E. F. Harrison, R. B. Lee III, G. L. Smith, and J. E. Cooper, Clouds and the Earth's Radiant Energy System (CERES): An Earth observing system experiment, *Bull. Am. Meteorol. Soc.*, *77*, 853–868, 1996.

Wiscombe, W. J., and G. W. Grams, The backscattered fraction in two-stream approximations, *J. Atmos. Sci.*, *33*, 2440–2451, 1976.

R. Bergstrom, S. Howard, J. Pommier, M. Rabbette, and B. Schmid, Bay Area Environmental Research Institute, Sanoma, CA, USA.

W. Gore and P. Pilewskie, Earth Science Division, National Aeronautics and Space Administration (NASA) Ames Research Center, Moffett Field, CA, USA. (ppilewskie@mail.arc.nasa.gov)

P. V. Hobbs, Department of Atmospheric Sciences, University of Washington, Seattle, WA, USA.

S. C. Tsay, National Aeronautics and Space Administration (NASA) Goddard Space Flight Center, Greenbelt, MD, USA.